Stabilization of High Oxidation States in Transition Metals. 2.[1] WCl_6 Oxidizes $[WF_6]^-$, but Would $PtCl_6$ Oxidize $[PtF_6]^-$? An Electrochemical and Computational Study of 5d Transition Metal Halides: $[MF_6]^z$ versus $[MCl_6]^z$ (M = Ta to Pt; z = 0, 1−, 2−)

Stuart A. Macgregor*,† and Klaus H. Moock*

Research School of Chemistry, Australian National University, Canberra ACT 0200, Australia

Received May 21, 1996

The trends in redox potentials for isovalent series of 5d hexafluoro- and -chlorometalates, $[MX_6]^{0/-}$ and $[MX_6]^{-/2-}$ (M = Ta to Pt; X = F, Cl), are compared, including the previously unpublished electrochemistry of $[IrF_6]^{2-}$. For a given series, the trend in redox data can be understood in terms of the core charge of the metal and interelectronic terms. However, there is a marked convergence of the electrochemical redox potentials for isovalent series of $[MF_6]^{z/z-1}$ and $[MCl_6]^{z/z-1}$ (z = 0, 1−) complexes. Thus, while the oxidation potential of $[TaF_6]^{2-}$ is 1.6 V lower than that of $[TaCl_6]^{2-}$, the oxidation potential of $[IrF_6]^{2-}$ is only 0.5 V lower than that of $[IrCl_6]^{2-}$. The redox data correlate well with computed electron affinities of MX_6 and $[MX_6]^-$ derived from density functional calculations. A fragmentation approach is adopted to analyze the electrochemical trends in terms of the properties of the metal center and trends in the metal−halide bonding. The observed convergence in redox data for isovalent $[MX_6]^{z/z-1}$ (x = F, Cl; z = 0, 1−) series is rationalized in terms of the ability of the halide arrays to stabilize the two metal oxidation states involved. The ability of the chloride array to stabilize the higher metal oxidation state increases more rapidly along the third row transition metals than does that of the fluoride array. This counteracts the effects of metal core charge to produce the observed convergence. The computational results indicate that, for the later metals in their highest oxidation states, the redox-active orbital becomes increasingly halide based. In view of this, the stability of the neutral hexahalides with respect to the reductive elimination of X_2 was studied, and the results suggest that $OsCl_6$ and $IrCl_6$ are more likely to be stable as novel hexachlorides than $PtCl_6$.

Introduction

Recently, we reported on octahedral and pseudo-octahedral molybdenum and tungsten complexes, $[MCl_6]^{0/-/2-}$, $[MF_6]^-$, $[MNCl_4]^-$, $[MOCl_5]^{2-}$, as well as the metalladithiatriazene, $[Cl_4M(N_3S_2)]^-$, and metallaphosphazene $[Cl_3M(N_3(PPh_2)_2)]$ complexes (M = Mo, W).[1] The electrochemical data of these compounds indicate a strong influence of the different ligand sets on the redox potentials, with the relative stability of the higher metal oxidation state following the order $Cl_6 < F_6 < Cl_5O < Cl_4(N_3S_2) < Cl_3(N_3(PPh_2)_2) < Cl_4N$. These results are in agreement with the generally held view that fluoride is more efficient at stabilizing high metal oxidation states than chloride.

In our previous study, density functional calculations were employed to compute the energy difference between the oxidized (d^0) and reduced (d^1) species in their optimized equilibrium geometries. The computed ionization energies obtained in this way qualitatively reproduced the trends in redox data, allowing us, through analysis of the electronic structure of the d^0 species, to relate the ease of oxidation of the corresponding d^1 system to the nature of the metal−ligand interactions. Comparing MCl_6, $[MOCl_5]^-$, and $[MNCl_4]^-$ (M = Mo, W), we found the stability of the d^0 (M^{VI}) system to correlate with the extent of electron donation from the axial ligands, $\{Cl\cdots Cl\}^{2-}$, $\{Cl\cdots O\}^{3-}$, and N^{3-}, respectively. However, the reasons for the easier oxidation of $[MF_6]^-$ compared to that of $[MCl_6]^-$ are more subtle and are related to the changes that occur in metal−halide bonding. Upon oxidation, both ionic and covalent interactions between the central metal and the halide array increase. Changes in covalent bonding are more significant for $[MCl_6]^-$, while changes in ionic bonding predominate in $[MF_6]^-$. The latter effect results in the higher oxidation state being more accessible for the hexafluoride.[1]

The differences in the redox potentials between the hexafluoro[2] and hexachloro[3] complexes of tungsten and molybdenum are well documented. However, the dependence of the stability of a high oxidation state MX_6 species (X = F, Cl) on the precise nature of the metal−halide interaction motivated us to broaden our inquiry to a wider series of third row transition metal fluoride and chloride complexes, $[MX_6]^{0/-/2-}$ (M = Ta to Pt). Such a wide-ranging comparison, the results of which are presented here, has not been previously reported.

In general, the neutral transition metal hexafluorides have received more attention in the literature than their hexachloride analogues, from both an experimental and a theoretical point of view. Interest in the hexafluorides is derived from the very

† Current address: Department of Chemistry, Heriot-Watt University, Riccarton, Edinburgh EH14 4AS, U.K.

(1) For part 1, see: Moock, K. H.; Macgregor, S. A.; Heath, G. A.; Derrick S.; Boeré, R. T. *J. Chem. Soc., Dalton Trans.* **1996**, 2067.

(2) (a) Moock, K. H.; Rock, M. H. *J. Chem. Soc., Dalton Trans.* **1993**, 2459. (b) Brownstein, S.; Heath, G. A.; Sengupta, A.; Sharp, D. W. A. *J. Chem. Soc., Chem. Commun.* **1983**, 669. (c) Anderson, G. M.; Iqbal, J.; Sharp, D. W. A.; Winfield, J. M.; Cameron, J. H.; McLeod, A. G. *J. Fluorine Chem.* **1984**, *24*, 303. (d) Heath, G. A.; Hefter, G. T.; Boyle, T. W.; Desjardins, C. D.; Sharp, D. W. A. *J. Fluorine Chem.* **1978**, *11*, 399. (e) Moock, K. H.; Turowsky, L.; Seppelt, K. *J. Fluorine Chem.* **1987**, *37*, 253. (f) Sengupta, A. K.; Sharp, D. W. A.; Heath, G. A.; Brownstein, S. *J. Fluorine Chem.* **1982**, *21*, 38.

(3) Heath, G. A.; Moock, K. H.; Sharp, D. W. A.; Yellowlees, L. J. *J. Chem. Soc., Chem. Commun.* **1985**, 1503.

S0020-1669(96)00573-3 CCC: $15.00
Published on Web 05/30/1998

high electron affinities of the neutral species and, hence, their utility as extreme oxidation agents. Since the classic work of Bartlett and co-workers,[4] the electron affinities of the neutral hexafluorides of the third transition series have been generally believed to increase regularly in the sequence $WF_6 < ReF_6 < OsF_6 < IrF_6 < PtF_6$. The available experimental data on the gas-phase electron affinities of neutral hexafluorides have been interpreted as confirming Bartlett's general conclusion of an increase in electron affinity from left to right along a transition metal row. However, these data, which have been determined using a variety of procedures, are subject to relatively large experimental errors.[5]

In contrast, electrochemical methods provide a convenient tool with which to assess the relative stabilities of hexahalometalate species in different oxidation states. Systematic studies of the transition metal hexafluoro[2b] and hexachloro[3] species have been undertaken previously. In these studies, the orderly, periodic trends in redox potentials were first observed for the hexafluorometalate series,[2b] while, at a later stage, with the examination of the more extensive data set of the hexachlorometalates, the orderly progressions of these trends were further defined.[3] However, to date, a detailed comparison of both sets of data has not been carried out. More recently, the redox potentials of $[NbX_6]^-$ and $[TaX_6]^-$ complexes (X = F, Cl, and $-OTeF_5$) have been compared, and the ability of these ligands to stabilize high oxidation states has been described.[6]

A number of theoretical studies on the electron affinities of the neutral 5d hexafluorides have been reported. These have mostly relied on the Xα methodology and have supported Bartlett's conclusion of a general *linear* increase in electron affinity from left to right along the third row transition metals.[7,8] Fewer calculations on the second electron affinities of hexafluoride species have been reported. Miyoshi and co-workers[9] calculated the first and second electron affinities for the hexafluorides of the Cr triad by ab initio methods. Gutsev and Boldyrev calculated a value of +0.7 eV for the second electron affinity of PtF_6.[8c] So far, no experimental or computed electron affinities are available for the neutral hexachlorides. In an early paper, Cotton and Harris[10] employed extended Hückel calculations to analyze the electronic structures of $[MCl_6]^{2-}$ species (M = Re to Pt). More recently, Frenking and co-workers[11] have used ab initio calculations to compare charge distributions in MoX_6 and WX_6 (X = F, Cl). Using similar methods, Gutowski and co-workers[12] have studied the properties of multiply charged anionic hexahalo systems, including a number of early transition metal complexes. Finally, Deeth and Jenkins[13] have used density functional calculations to compute geometries and heterolytic M-Cl bond energies for a number of second and third row transition metal $[MCl_6]^{2-}$ systems.

In this work, we shall initially present the available electrochemical data on these extended series of hexafluoro- and hexachlorometalates, including the previously unreported data for $[IrF_6]^{2-}$. We then employ density functional calculations to model trends in the redox data through computation of what are effectively the gas-phase electron affinities of metal hexafluoro and hexachloro species. The computed results provide a framework in which the factors underlying the experimental trends can be understood.

Experimental Section

Electrochemical techniques and equipment have been described in detail previously.[1,2a] Where necessary, operations were carried out in a Pyrex vacuum line or an argon-filled glovebox (MBraun). Reaction vessels were flamed out prior to use under vacuum. MeCN (Merck, analytical grade) was purified and dried according to a literature method.[14] CH_2Cl_2 (Aldrich, analytical grade) was refluxed over P_2O_5 for 1 h and then distilled into a round-bottomed flask containing activated 3-Å molecular sieves. The solvent was immediately degassed on a vacuum line (freeze−thaw method) and subsequently protected from light.

Hexachlorometalates. The complexes $[NBu_4]_2[HfCl_6]$,[15] $[NBu_4][TaCl_6]$,[16] $[NBu_4][WCl_6]$,[17] and $[NBu_4]_2[ReCl_6]$[18] were synthesized by adaptation of literature procedures. The metal chlorides $HfCl_4$, $TaCl_5$, WCl_6, and $ReCl_5$ were freed from oxochloride impurities by fractional sublimation in a sealed Pyrex tube. Cation-exchange reactions with NBu_4Cl (Fluka AG) were carried out in double-limb vessels fitted with Rotaflo stopcocks, and the solvent, CH_2Cl_2, was vacuum transferred. $[NBu_4]_2[OsCl_6]$, $[NBu_4]_2[IrCl_6]$, and $[NBu_4]_2[PtCl_6]$ were precipitated from their commercially available potassium salts (Aldrich, Johnson Matthey) with NBu_4Cl in 1 N HCl solutions, washed with a small amount of cold acetone, and dried in vacuo.

Hexafluorometalates. The salts of $[WF_6]^-$ [2a,e] were prepared by literature methods. $K[IrF_6]$ was prepared in a silica vessel by reacting a mixture of Ir_2Br_7/KBr with an excess of BrF_3 (Air Products).[19] After the release of bromine, excess BrF_3 was removed with the help of a metal vacuum line at 180 °C. Hydrolysis with a minimum amount of water at 60 °C afforded, after filtration to remove iridium hydroxide and crystallization from distilled water, yellow plates of $K_2[IrF_6]$.[19] The free acid of the hexafluoroiridate(IV), $H_2[IrF_6]\cdot nH_2O$, was prepared by passing $K_2[IrF_6]$, dissolved in the minimum amount of distilled water, through an exchange column in the hydrogen form (Amberlite IR 120).[20] The pH of the resulting solution was typically between 1.5 and 2.0. $Na_2[IrF_6]$ and $[NBu_4]_2[IrF_6]$ were formed by neutralizing the free acid with the stoichiometric amount of 0.005 N NaOH or NBu_4OH, respectively, while stirring vigorously to avoid local concentrations of OH^-. The pH of the solutions was maintained between 3.5 and 4.0 since neutralization to pH 7 results in decomposition of the $[IrF_6]^{2-}$ anion and formation of iridium hydroxide. Removal of water under vacuum at room temperature resulted in either air-stable white microcrystals of $Na_2[IrF_6]$ or metallic shining platelets of $[NBu_4]_2[IrF_6]$.

(4) (a) Bartlett, N.; Beaton S. P.; Jha, N. K. *J. Chem. Soc., Chem. Commun.* **1966**, 168. (b) Bartlett, N. *Angew. Chem., Int. Ed. Engl.* **1968**, *7*, 433.
(5) (a) Korobov, M. V.; Kuznetsov, S. V.; Sidorov, L. N.; Shipachev, V. A.; Mit'kin, V. N. *Int. J. Mass. Spectrom. Ion Processes* **1989**, *87*, 13. (b) Sidorov, L. N.; Borshchevsky, A. Ya.; Rudny, E. B.; Butsky, V. D. *Chem. Phys.* **1982**, *71*, 145. (c) Sidorov, L. N. *Usp. Khim.* **1982**, *51*, 625. (d) George, P. M.; Beauchamp, J. L. *Chem. Phys.* **1979**, *36*, 345. (e) Burgess, J.; Haigh, I.; Peacock, R. D.; Taylor, P. *J. Chem. Soc., Dalton Trans.* **1974**, 1064. (f) Compton, R. N.; Reinhardt, P. W.; Cooper, C. D. *J. Chem. Phys.* **1978**, *68*, 2023.
(6) Moock, K. H.; Seppelt, K. *Z. Anorg. Allg. Chem.* **1988**, *561*, 132.
(7) Bloor, J. E.; Sherrod, R. E. *J. Am. Chem. Soc.* **1980**, *102*, 4333.
(8) (a) Gutsev, G. L.; Boldyrev, A. I. *Chem. Phys. Lett.* **1983**, *101*, 441. (b) Gutsev, G. L.; Boldyrev, A. I. *Adv. Chem. Phys.* **1985**, *61*, 169. (c) Gutsev, G. L.; Boldyrev, A. I. *J. Phys. Chem.* **1990**, *94*, 2256.
(9) Miyoshi, E.; Sakai, Y.; Murakami, A.; Iwaki, H.; Terashima, H.; Shoda, T.; Kawaguchi, T. *J. Chem. Phys.* **1988**, *89*, 4193.
(10) Cotton, F. A.; Harris, C. B. *Inorg. Chem.* **1967**, *6*, 376.
(11) Neuhaus, A.; Veldkamp, A.; Frenking, G. *Inorg. Chem.* **1994**, *33*, 5278.
(12) (a) Rak, J.; Gutowski, M.; Dokurno, P.; Vu Thanh, H.; Blazejowski, J. *J. Chem. Phys.* **1994**, *100*, 5810. (b) Gutowski, M.; Boldyrev, A. I.; Ortiz, J. V.; Simons, J. *J. Am. Chem. Soc.* **1994**, *116*, 9262. (c) Gutowski, M.; Boldyrev, A. I.; Simons, J. Rak, J.; Blazejowski, J. *J. Am. Chem. Soc.* **1996**, *118*, 1173.
(13) Deeth, R. J.; Jenkins, H. D. B. *J. Phys. Chem. A.* **1997**, *101*, 4793.
(14) Winfield, J. M. *J. Fluorine Chem.* **1984**, *25*, 91.
(15) van Bronswyk, W.; Clark, R. J. H.; Maresca, L. *Inorg. Chem.* **1969**, *8*, 1395.
(16) Brisdon, B. J.; Fowles, G. W. A.; Tidmarsh, D. J.; Walton, R. A. *Spectrochim. Acta* **1969**, *A25*, 999.
(17) Dickenson, R. N.; Feil, S. E.; Collier, F. N.; Horner, W. W.; Horner, S. M.; Tyree, S. Y. *Inorg. Chem.* **1964**, *3*, 1600.
(18) Tisley, D. G.; Walton, R. A. *J. Chem. Soc. (A)* **1971**, 3409.
(19) Hepworth, M. A.; Robinson P. L.; Westland, G. J. *J. Chem. Soc.* **1954**, 4269.
(20) Hepworth, M. A.; Robinson P. L.; Westland, G. J. *J. Chem. Soc.* **1958**, 611.

Computational Details

Calculations employed the Amsterdam Density Functional (ADF) package developed by Baerends and co-workers[21] and the numerical integration scheme of te Velde and Baerends.[22] Triple-ζ STO basis sets were employed for all metal atoms, and double-ζ STO basis sets extended with a polarization function were used for Cl and F.[23] An auxiliary set of s, p, d, f, and g STO basis functions centered on all nuclei was used in order to fit the molecular density and describe accurately the Coulomb and exchange potentials in each SCF cycle.[24] Core electrons (up to and including 5p for the metals, 2p for Cl, and 1s for F) were treated using the frozen core approximation. The local density approximation[25] (LDA) was employed using the parametrization of Vosko et al.[26] Geometry optimization was performed at the LDA level by the method developed by Versluis and Ziegler[27] and included the quasi-relativistic correction of Ziegler et al.[28] The energies of all LDA-optimized species were recalculated to include the nonlocal gradients corrections of Becke[29] and Perdew.[30] Spin-polarized, unrestricted calculations were performed on all open-shell species. The open-shell method[31] was employed in the fragment calculations of all open-shell systems.

The electron affinities of hexahalometalates are the negative of the energy for the process:

$$[MX_6]^{n-} + e \rightarrow [MX_6]^{(n+1)-}$$

A positive electron affinity, therefore, corresponds to stabilization upon electron addition. As we are concerned with modeling electrochemical redox processes, we have chosen to compute optimized structures for both the $[MX_6]^{n-}$ and $[MX_6]^{(n+1)-}$ species, allowing us to take full account of the effects of geometric relaxation upon electron addition. Comparison of the energies of these species then yields the $[MX_6]^{n-}$ electron affinity according to the above equation.

Results

1. Electrochemistry. The electrochemical potentials of $[NBu_4]_2[IrF_6]$ recorded in CH_2Cl_2 and MeCN as well as those of $Na_2[IrF_6]$ in DMSO have been established by voltammetric methods. All redox potentials are reported versus the saturated calomel electrode (SCE). In all three solvents, the one-electron oxidation process, $[IrF_6]^{-/2-}$ (d^4/d^5), is reversible at ambient temperature, with $E_{1/2} = +1.23$ (CH_2Cl_2), +1.29 (MeCN), and +1.46 V (DMSO). However, only in CH_2Cl_2 is the reduction process, $[IrF_6]^{2-/3-}$ (d^5/d^6), quasi-reversible at $E_{1/2} = -1.48$ V. In MeCN and DMSO, this reduction process is strictly irreversible, even at low temperatures and faster scan rates (up to 5 V s^{-1}), with an anodic peak-to-peak separation of 2.8 (MeCN) and 3.2 V (DMSO). The irreversible behavior can be attributed to an EC mechanism in which the reduced species reacts with the strongly coordinating MeCN and DMSO solvents. Figure 1 compares the cyclic voltammograms (cv) and alternating current voltammograms (acv) of $[NBu_4]_2[IrF_6]$ and $[NBu_4]_2[IrCl_6]$ in CH_2Cl_2.

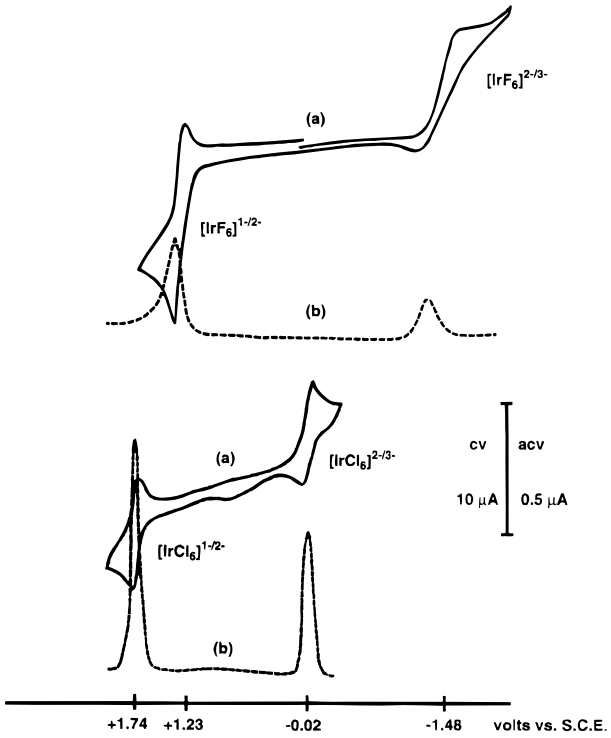

Figure 1. Comparison of cyclic voltammograms (a) and alternating current voltammograms (b) of $[NBu_4]_2[IrF_6]$ and $[NBu_4]_2[IrCl_6]$ in CH_2Cl_2 at a Pt electrode. Scan rates: 50 (cv) and 20 mV s^{-1} (acv).

The experimental redox data for $[IrF_6]^{2-}$ are shown in Table 1, along with the redox potentials reported previously for the extended series of 5d hexafluoro- and hexachlorometalates, recorded in MeCN and CH_2Cl_2, respectively (see Table 1 for conditions). The redox potentials of these hexahalometalates measured in these solvents do not differ by more than 0.07 V, except, as was the case for $[IrF_6]^{2-}$, where the complexes react with the solvent. The bulk of these experimental redox data have been reexamined and the potentials confirmed to within 0.02 V. All redox processes corresponded to reversible, or quasi-reversible, one-electron steps according to

$$[MX_6]^z + e \rightleftharpoons [MX_6]^{z-1}$$

$$(M = \text{Hf to Pt};\ X = \text{F or Cl};\ z = 0, 1-, 2-)$$

The trends in redox data for the $[MX_6]^{0/-}$ and $[MX_6]^{-/2-}$ couples are displayed in Figure 2.

2. Computational Results. Optimized Geometries. All the hexahalo species have been treated as regular octahedra. Although many of the systems studied are, in principle, subject to Jahn−Teller distortions as a result of electronic degeneracy within the t_{2g} set, this effect is expected to be small.[32] The optimized M−X distances are given in Table 2, together with the available experimental data. As found previously,[1] we compute M−X distances to be somewhat longer than those determined experimentally. In general, there is a tendency for a decrease in M−X distance with increasing metal core charge.

(21) (a) Baerends, E. J.; Ellis, D. E.; Ros, P. *Chem. Phys.* **1973**, *2*, 41. (b) Baerends, E. J. In *Chemistry and Solid State Physics*; Dahl, J. P., Avery, J., Eds., Plenum: New York, 1984.
(22) te Velde, G.; Baerends, E. J. *J. Comput. Phys.* **1992**, *99*, 84.
(23) (a) Snijders, G. J.; Baerends, E. J.; Vernooijs, P. *At. Data Nucl. Data Tables* **1982**, *26*, 483. (b) Vernooijs, P.; Snijders, G. J.; Barends, E. J. *Slater Type Basis Functions for the hole Periodic System*; Internal Report; Free University of Amsterdam: Amsterdam, The Netherlands, 1981.
(24) Krijn, J.; Baerends, E. J. *Fit Functions in the HFS-method*; Internal Report; Free University of Amsterdam: Amsterdam, The Netherlands, 1984.
(25) (a) Gunnarsson, O.; Lundqvist, B. I.; Wilkins, J. W. *Phys. Rev. B* **1974**, *10*, 1319. (b) Gunnarsson, O.; Lundqvist, B. I. *Phys. Rev. B* **1976**, *13*, 4274. (c) Gunnarsson, O.; Jonson, M.; Lundqvist, B. I. *Phys. Rev. B* **1979**, *20*, 3136.
(26) Vosko, S. H.; Wilk, L.; Nusair, M. *Can. J. Phys.* **1980**, *58*, 1200.
(27) Versluis, L.; Ziegler, T. *J. Chem. Phys.* **1988**, *88*, 322.
(28) (a) Ziegler, T.; Tschinke, V.; Baerends, E. J.; Snijders, J. G.; Ravenek, W. *J. Phys. Chem.* **1989**, *93*, 3050. (b) van Leeuwen, R.; van Lenthe, E.; Snijders, J. G.; Baerends, E. J. *J. Chem. Phys.* **1994**, *101*, 1272.
(29) Becke, A. D. *J. Chem. Phys.* **1986**, *84*, 4524.
(30) Perdew, J. P. *Phys. Rev. B* **1986**, *33*, 8822.
(31) Bickelhaupt, F. M.; Nibbering, N. M. M.; van Wezenbeck, E. M.; Baerends, E. J. *J. Phys. Chem.* **1992**, *96*, 4864.
(32) Gillespie, R. J. *J. Chem. Educ.* **1970**, *47*, 18.

Table 1. Electrochemical Data for Hexahalometalates in Volts vs SCE

(a) Hexafluorometalates[a]

metal	$[MF_6]^{0/-}$	$[MF_6]^{-/2-}$	$[MF_6]^{2-/3-}$
Ta[b]		−2.17	
W[c]	+1.06	−0.93	
Re[b]	+2.38	+0.18	
Os[b]	+3.28	+0.63	−1.92
Ir		+1.29	−1.5[d]
Pt		+1.84[e]	

(b) Hexachlorometalates[f]

metal	$[MCl_6]^{0/-}$	$[MCl_6]^{-/2-}$	$[MCl_6]^{2-/3-}$
Hf			−3.1[g]
Ta		−0.55[h]	−2.05[i]
W[j]	+1.59	+0.40	−1.15
Re	+2.35[k]	+1.33[h]	−1.12[l]
Os[m]	+3.1[e]	+1.28[h]	−0.64[h]
Ir[n]		+1.74[h]	−0.02[h]
Pt		+2.30[o]	

[a] At a platinum electrode in MeCN containing 0.1 mol NEt_4PF_6, referenced to SCE such that $E_{1/2} = +0.38$ V for $[Cp_2Fe]^{+/0}$. [b] From ref 2b,f. [c] From refs 1, 2a. In CH_2Cl_2, $E_{1/2} = +1.08$ V for $[WF_6]^{0/-}$ and −0.91 V for $[WF_6]^{-/2-}$.[2e] [d] Irreversible behavior in MeCN; anodic peak potential (E_a). [e] Extrapolated potential. [f] At a platinum electrode in CH_2Cl_2 containing 0.5 mol of NBu_4PF_6, referenced to SCE such that $E_{1/2} = +0.48$ V for $[Cp_2Fe]^{+/0}$. [g] Extrapolated potential outside solvent range. [h] Reversible conditions also confirmed by ac voltammetry. [i] Separation of anodic (E_a) and cathodic (E_c) peak = 120 mV at −35 °C. [j] From ref 1. [k] $E_a - E_c = 75$ mV at −40 °C. [l] $E_a - E_c = 100$ mV at −40 °C. [m] In MeCN, $E_{1/2} = +1.24$ V for $[OsCl_6]^{-/2-}$ and −0.68 V for $[OsCl_6]^{2-/3-}$.[41] [n] In MeCN, $E_{1/2} = +1.67$ V for $[IrCl_6]^{-/2-}$ and −0.04 V for $[IrCl_6]^{2-/3-}$.[41] [o] $E_a - E_c = 90$ mV at −35 °C.

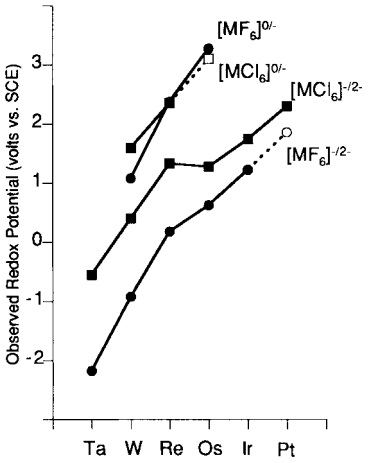

Figure 2. Trends in half-wave potentials, $E_{1/2}$ in volts, of $[MX_6]^{z/z-1}$ (M = Ta to Pt; X = F, Cl; $z = 0, 1-$) couples. Open markers refer to extrapolated data (see Table 1).

This tendency is much reduced in the later metals, and our calculations, in fact, predict a lengthening of the M−X bond between Ir and Pt for all six series. Whether this is an artifact of the computational method is not clear: unfortunately, there are insufficient experimental data to corroborate this finding. However, where it is possible to discern trends in the experimental data, they are reproduced in the computed results. For example, the M−F distances in WF_6, OsF_6, and IrF_6, as determined by electron diffraction, are within 0.003 Å of each other, while the computed M−F distances of these species fall in a similarly narrow range (1.882−1.887 Å). In addition, the steady increase in W−Cl distance in the $[WCl_6]^{0/-/2-}$ family upon reduction is reproduced by our calculations, as is the shortening of the M−Cl distance from Hf to Os in the $[MCl_6]^{2-}$ series.

Table 2. Computed M−X Bond Distances (Å) (Average Experimental Data in Parentheses)

(a) Hexafluorometalates

metal	MF_6	$[MF_6]^-$	$[MF_6]^{2-}$
Hf			2.068
Ta		1.957 (1.84[a])	2.038
W	1.886 (1.833[b])	1.943	2.019
Re	1.882	1.934	2.010 (1.953[c])
Os	1.882 (1.831[b])	1.928	1.997
Ir	1.887 (1.830[b])	1.927	1.990
Pt	1.903	1.937	1.991

(b) Hexachlorometalates

metal	MCl_6	$[MCl_6]^-$	$[MCl_6]^{2-}$
Hf			2.518 (2.448[d])
Ta		2.402 (2.33[e])	2.469
W	2.333 (2.289[f])	2.374 (2.33[g])	2.434 (2.383[h])
Re	2.322	2.357 (2.267[i])	2.411 (2.361[j])
Os	2.317	2.344 (2.284[k])	2.387 (2.332[k])
Ir	2.324	2.344	2.379
Pt	2.341	2.353	2.380 (2.328[l])

[a] McLoughlin, M. A.; Keder, N. L.; Kaska, W. C. *Acta Crystallogr. C.* **1992**, *48*, 1098. [b] Kimura, M.; Schomaker, V.; Smith, D. W.; Weinstock, B. *J. Chem. Phys.* **1968**, *48*, 4001. [c] Clark, G. R.; Russell, D. R. *Acta Crystallogr.* **1978**, *B34*, 894. [d] Beck, J.; Biedenkopf, P.; Müller-Buschbaum, K.; Richter, J.; Schlitt, K−J. *Z. Anorg. Allg. Chem.* **1996**, *622*, 292. [e] Preiss, H. *Z. Anorg. Allg. Chem.* **1971**, *380*, 56. [f] Strand, T. R. *Acta Chim. Scand.* **1994**, *48*, 960. [g] Eichler, W.; Seifert, H−J. *Z. Anorg. Allg. Chem.* **1977**, *431*, 123. [h] Roesky, H. W.; Mainz, B.; Noltemeyer, M.; Sheldrick, G. M. *Z. Naturforsch. B* **1988**, *43*, 941. [i] Arp, O.; Preetz, W. *Z. Anorg. Allg. Chem.* **1994**, *620*, 1391. [j] Lisher, E. J.; Cowlam, N.; Gilliot, *L. Acta Crystallogr.* **1979**, *B35*, 1033. [k] Kim, E. U.; Eriks, K.; Magnuson, R. *Inorg. Chem.* **1984**, *23*, 393. [l] Viossat, B.; Hourfar, A.; Rodier, N. *Bull. Soc. Chim. Fr.* **1981**, 454.

Table 3. Computed Electron Affinites for Neutral Hexahalides, MX_6 (M = Ta to Pt; X = F, Cl) (Results Are Compared with Those Derived from Experiment and Previous Theoretical Studies)

	MF_6				MCl_6,
M	experimental	this work	DV-Xα[a]	ab initio[b]	this work
W	3.51 ± 0.1[c]	3.34	3.5	3.85	4.11
Re		4.50	4.8		4.88
Os	5.93 ± 0.28[d]	5.55	6.0		5.52
Ir	6.50 ± 0.38[d]	5.34	5.8[e] (7.2)		5.34
Pt	7.00 ± 0.35[d]	6.36	6.9[e] (7.4)		5.98

[a] Reference 8a. [b] Reference 9. [c] Reference 5c. [d] Reference 5a. [e] High-spin results calculated using data in ref 8a. Figures in parentheses were calculated using a low-spin electronic configuration and are as quoted in Figure 8a.

Table 4. Computed Electron Affinities (eV) of $[MX_6]^-$ Species (M = Ta to Pt; X = F, Cl)

metal	$[MF_6]^-$	$[MCl_6]^-$	metal	$[MF_6]^-$	$[MCl_6]^-$
Ta	−4.14	−1.40	Os	−2.34	−0.23
W	−2.98	−0.54	Ir	−1.22	+0.53
Re	−1.81	+0.26	Pt	−0.10	+1.28

Computed Electron Affinities. Computed electron affinities for MX_6 and $[MX_6]^-$ species are given in Tables 3 and 4, respectively, and are plotted together in Figure 3. Comparison with Figure 2 indicates that our computed electron affinities reproduce the nonlinear progression observed for the experimental redox data for the $[MX_6]^{-/2-}$ couple. In addition, the convergence observed for the redox data for the $[MF_6]^{-/2-}$ and $[MCl_6]^{-/2-}$ series is clearly reproduced by the calculated electron affinities of $[MX_6]^-$ species. For the $[MX_6]^{0/-}$ couple, the convergence of the fluoro- and chloro experimental data between W and Os is, again, well reproduced, while our calculations predict that a

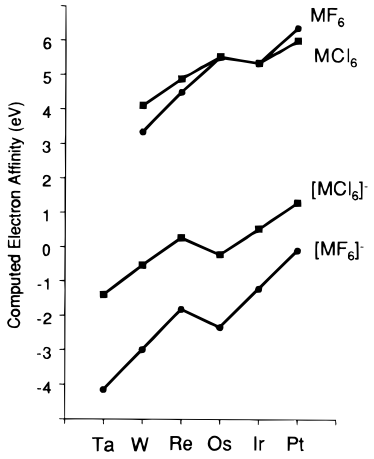

Figure 3. Trends in computed electron affinities (electronvolts) of $[MX_6]^z$ (M = Ta to Pt; X = F, Cl; $z = 0, 1-$) species.

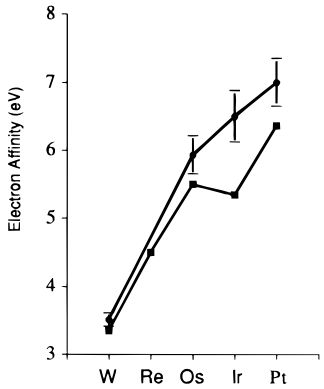

Figure 4. Comparison of computed and available experimentally determined electron affinities (electronvolts) for MF_6 species (M = W to Pt).

discontinuity in redox data would occur between $[OsX_6]^{0/-}$ (d^2/d^3) and $[IrX_6]^{0/-}$(d^3/d^4). Our calculated electron affinities for the 5d neutral hexafluorides are compared with the available experimental gas-phase electron affinities in Figure 4, while the results of both previous theoretical and experimental studies are given in Table 3. In general, our computed values are slightly lower than the experimental results. We postpone further comparison of our results with these experimental electron affinities and previous theoretical treatments to the Discussion, but note at this point the relatively high error bars associated with the experimental data. The computed electron affinities of the MF_6 and MCl_6 species, in fact, cross in the later MX_6 species (Figure 3). This reversal of MX_6 electron affinities is consistent with the available electrochemical data for the neutral hexahalides (Table 1): the $E°$ values for the reduction of ReF_6 and $ReCl_6$ are effectively the same, and extrapolation of the data for WX_6 and OsF_6, following the trends seen in the $M^{V/IV}$ couple, would predict a more positive reduction potential (corresponding to a higher electron affinity) for PtF_6 compared to that for $PtCl_6$. In other words, PtF_6 should be a stronger oxidizing agent than the hypothetical $PtCl_6$. This is an unexpected result, as fluoride is generally considered to be more effective at stabilizing high oxidation states than chloride.

Discussion

1. Trends in Redox Data and Computed Electron Affinities for Hexahalometalates. The redox data for the $[MX_6]^{-/2-}$ couple (X = F, Cl) across the third row transition metals display an increasing ease of reduction, which is

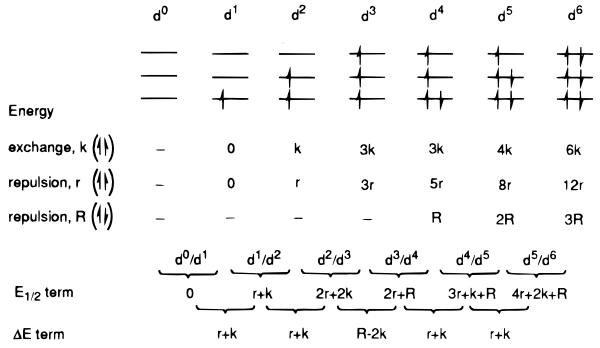

Figure 5. Interelectronic correlation terms for octahedral complexes.

interrupted at the d^3/d^4 couple to produce a nonlinear ("zigzag") pattern. The general increase in the ease of reduction has been interpreted as resulting from the higher core charge of the metal, which is inefficiently shielded by the d-electrons.[4,7] The discontinuity at the d^3/d^4 couple arises from interelectronic repulsion terms.[2b] Across the third row transition metal series, the change in electronic configuration in octahedral complexes is, to a first approximation, confined to the metal-based t_{2g} orbitals. Since the t_{2g} orbitals can be considered ideally degenerate, the contribution of interelectronic repulsion terms to the separation between couples $E(d^{n-1}/d^n)$ and $E(d^n/d^{n+1})$ should be uniformly $[r + k]$ for $n = 1$, 2, 4, and 5 but $[R - 2k]$ for $n = 3$, where r is the repulsion energy between any two electrons in different orbitals, k is the exchange energy between any two parallel electrons, and R is the repulsion energy for electrons paired within one orbital.[2b] Figure 5 shows how consideration of these interelectronic terms leads to the observed pattern in redox data as the t_{2g} manifold is filled. If, as in the preceding argument, the experimental redox data depended solely on the occupation of the metal d-orbitals, the same potentials would be obtained independent of the surrounding ligands. However, this will not be generally true, as metal−ligand interactions result in delocalization of the metal d-orbitals onto the ligands (illustrated by the nephelauxetic effect[33]). The trends in experimental redox data will, therefore, depend on the nature of the metal-to-halide interaction.

A direct comparison of the trends in redox potentials of the third row hexafluoro- and hexachlorometalates for the $[MX_6]^{-/2-}$ couple (Figure 2) illustrates these ideas. For both halides, the expected trend is observed, with a linear increase in reduction potential for M = Ta to Re (d^0/d^1 to d^2/d^3) and M = Os to Pt (d^3/d^4 to d^5/d^6). The discontinuity between the $Re^{V/IV}$ and $Os^{V/IV}$ couples arises from the exchange repulsion that occurs in the d^4 $[OsX_6]^{2-}$ species. The discontinuity is more pronounced for the $[MCl_6]^{-/2-}$ series; nevertheless, the effect of exchange repulsion is still important for the $[MF_6]^{-/2-}$ series. Linear extrapolation of the data for the $[MF_6]^{-/2-}$ couples (M = Ta, W, Re) predicts values for the $[OsF_6]^{-/2-}$ and $[IrF_6]^{-/2-}$ couples of +1.4 and +2.6 V, respectively, 0.8 and 1.3 V higher than their observed potentials. The addition of the redox potential for the $[IrF_6]^{-/2-}$ couple to the data set is, therefore, important, as it confirms that this nonlinear progression exists for both hexafluoro- and hexachlorometalate series.

The trends in the computed electron affinities of $[MX_6]^-$ species are shown in Figure 3. The nonlinear progression arising from the effects of exchange repulsion described above for the redox data is clearly reproduced, but, for reasons that are as yet unclear, the calculations fail to model the smaller discontinuity in the experimental data for the $[MF_6]^{-/2-}$ series. Despite

(33) Schäffer C. E.; Jørgensen C. K. *J. Inorg. Nucl. Chem.* **1958**, *8*, 143.

this, we can use the computational results to predict trends in redox behavior in systems that may be inaccessible by experimental electrochemical means. Thus, although there are not sufficient experimental data available to display the full zigzag pattern for the $[MX_6]^{0/-}$ couple (due to the extreme redox potentials that would be required), the computed electron affinities of MX_6 species display the expected trend, with the discontinuity occurring at the reduction of d^3 IrX_6. As was observed in the redox data for the $[MX_6]^{-/2-}$ couple, it is possible that the discontinuity in the $[MF_6]^{0/-}$ series would be less pronounced than that of the $[MCl_6]^{0/-}$ series. Although the electron affinity of IrF_6 may, therefore, be somewhat greater than that of OsF_6, overall we still do not expect a smooth linear trend. This conclusion is at odds with the interpretation of the available experimental gas-phase electron affinities, which have been used to support a general linear increase in electron affinity across the third row neutral hexafluorides. Figure 4 indicates that the errors associated with these experimental electron affinities are quite high and might easily obscure the type of nonlinear, zigzag trend described here, especially if it resembled that observed for the electrochemistry of the $[MF_6]^{-/2-}$ couple. Even given these large experimental errors, it is not possible to draw a straight line through the available experimental data once the experimentally determined electron affinity of WF_6 is taken into account. However, it should be noted that the WF_6 result is derived from a different study, employing a different methodology, from that of the other MF_6 species. From this point of view, the redetermination of MF_6 gas-phase electron affinities, including ReF_6, employing a similar methodology throughout, would be particularly useful.

The zigzag progression of electron affinity along the third row hexafluorides can be inferred from a previous DV-Xα study of the electron affinities of $[MF_6]^-$ species.[8a] In this study, electron affinities were derived from ionization potential calculations using the transition state method, involving removal of half an electron from the orbital involved. For d-electron counts greater than 3, the half electron removed may be of α or β spin, yielding either "high-spin" or "low spin" electron configurations.[34] The high-spin results give a zigzag trend similar to that calculated here. The low-spin configurations do result in a linear trend in electron affinity from WF_6 to IrF_6, although this trend does not extend to PtF_6. The calculated difference in electron affinity for low-spin and high-spin IrF_6 in this study is 1.4 eV. Despite this large difference, the low-spin results have been emphasized in subsequent treatments of MF_6 electron affinities.[5a,8b] Both the high-spin and low-spin results derived from this DV-Xα study are given in Table 3. Our computed electron affinities for MF_6 species are similar to those derived from ab initio calculations (M = W) and the high-spin DV-Xα method (M = W to Pt). The assumption of maximum multiplicity within the t_{2g} set in the calculations for IrF_6 and PtF_6 in our study leads to a larger discrepancy with the low-spin DV-Xα electron affinities for these species. However, as our calculations correctly reproduce the nonlinear progression of redox potentials across the 5d hexahalometalates, this assumption must better reflect the electronic structure of these species, at least in solution.

(34) Note that the high-spin and low-spin terminology used here should not be confused with that commonly employed to describe high-spin and low-spin electonic configurations resulting from the different occupations of the metal-based t_{2g} and e_g orbitals. Rather, it refers to the total spin of the species computed in the transition-state calculations. Thus, for d^4 $[IrF_6]^-$ with the electronic configuration $(t_{2g})^{3\alpha}(t_{2g})^{1\beta}$, the half electron removed can either be of α spin, yielding the "low-spin" transition state configuration, $(t_{2g})^{2.5\alpha}(t_{2g})^{1\beta}$, approximating d^3 IrF_6 with a final $(t_{2g})^{2\alpha}(t_{2g})^{1\beta}$ electron configuration, or of β spin, yielding the "high-spin" transition state configuration $(t_{2g})^{3\alpha}(t_{2g})^{0.5\beta}$, approximating d^3 IrF_6 with a final $(t_{2g})^{3\alpha}(t_{2g})^{0\beta}$ electron configuration.

Table 5. Calculated d-Orbital Occupations, Metal Charges, and Metal Character (%) in M−X Antibonding t_{2g} Orbitals in $[MX_6]^-$ Species (M = Ta to Pt; X = F, Cl)

		Ta	W	Re	Os	Ir	Pt
d-Orbital Occupation							
$[MF_6]^-$	$2t_{2g}$	0.00	0.75	1.43	1.99	2.28	2.15
	$1t_{2g}$	1.23	1.32	1.51	1.91	2.52	3.41
	e_g	0.90	1.04	1.16	1.24	1.44	1.76
total		2.13	3.11	4.10	5.14	6.24	7.31
$[MCl_6]^-$	$2t_{2g}$	0.00	0.66	1.24	1.63	1.72	1.35
	$1t_{2g}$	1.32	1.56	1.91	2.51	3.29	4.32
	e_g	1.44	1.48	1.60	1.84	2.12	2.52
total		2.76	3.70	4.75	5.98	7.13	8.19
Calculated Metal Charges							
$[MF_6]^-$		2.37	2.32	2.30	2.31	2.22	2.20
$[MCl_6]^-$		1.38	1.30	1.19	1.13	1.02	0.99
Metal Character (%) in $2t_{2g}$ (M−X Antibonding) Orbitals							
$[MF_6]^-$		77.7	75.2	71.7	66.3	57.0	42.9
$[MCl_6]^-$		69.8	66.1	61.8	54.4	42.9	27.0

While the shapes of the individual plots of redox data for an isovalent series of a given halide are well understood, we note a marked convergence of the plots for the fluoride and chloride series. For the $[MX_6]^{-/2-}$ couple, the gap between X = F and Cl is 1.62 V for M = Ta, but this decreases to 0.51 V for M = Ir and, by extrapolation, should be around 0.4 V for M = Pt. A similar convergence is also observed for the $[MX_6]^{0/-}$ couple. The redox potentials of $[ReF_6]^{0/-}$ and $[ReCl_6]^{0/-}$ are almost identical (+2.38 and +2.35 V, respectively), and linear extrapolation of the available hexafluoride and hexachloride data suggests that the $[OsCl_6]^{0/-}$ couple should appear at a lower potential than the $[OsF_6]^{0/-}$ couple at +3.28 V. This convergence of the redox data for isovalent hexafluoride and hexachloride series is discussed in the next section.

2. Convergence of Redox Data in $[MX_6]^{-/2-}$ Series (X = F, Cl). We concentrate in this section on the redox trends of the $[MX_6]^{-/2-}$ series, as these form the most complete experimental data set for the fluoride/chloride comparison. These data have been modeled by calculating the electron affinities of $[MX_6]^-$ species, and we shall, therefore, initially attempt to relate the trends in electron affinities to changes in the electronic structure of these M^V species. In particular, the nature of the $2t_{2g}$ acceptor orbital has been used as a means to rationalize trends in the electron affinities of neutral hexafluorides,[8,9] and we shall assess this approach in light of the data on both hexafluoro- and hexachlorometalates.

Table 5 lists calculated metal charges, total metal d-orbital occupations, and the percentage metal character in the $2t_{2g}$ acceptor orbitals for $[MX_6]^-$ species. The total metal d-orbital occupations arise from contributions from the $1e_g$ (metal−halide σ-bonding), $1t_{2g}$ (metal−halide π-bonding), and $2t_{2g}$ (metal−halide π-antibonding) orbitals as indicated. If we consider the $[WX_6]^-$ pair, both the lower calculated metal charge and the higher total metal d-orbital population in $[WCl_6]^-$ are consistent with chloride being a better donor than fluoride in these systems and suggest, contrary to both the redox data and the computed electron affinities, that electron addition to $[WCl_6]^-$ might be more difficult than that to $[MF_6]^-$. Comparing the $2t_{2g}$ acceptor orbitals of the $[WX_6]^-$ pair, we compute a lower degree of metal character in $[WCl_6]^-$, consistent with a stronger metal−halide antibonding interaction in this case. The $2t_{2g}$ acceptor orbital might, therefore, be considered to lie to higher energy in $[WCl_6]^-$ than in $[WF_6]^-$, and, on this basis alone, occupation

of this orbital would be harder for $[WCl_6]^-$. Once again, this is at odds with the experimental and computational data. On the other hand, the greater delocalization of the $2t_{2g}$ acceptor orbital in $[WCl_6]^-$ and the consequent lower degree of electron density at the metal (0.66 e compared to 0.75 e in $[WF_6]^-$), suggests that an extra electron may experience lower electronic repulsion in the reduced form of the chloride. This calculated parameter at least does appear consistent with the greater electron affinity of $[WCl_6]^-$ compared to that of $[WF_6]^-$.

We now examine trends in the electronic structures of the third row $[MX_6]^-$ species. The data in Table 5 are consistent with a general increase in metal−halide covalent interaction from left to right along the series. This can be understood in terms of a stabilization of the metal-based orbitals arising from the increased metal core charge and the consequent reduction in the energy mismatch between the halide donor levels and the metal-based orbitals. Calculated metal charges, therefore, show a steady decrease from Ta to Pt for both halides, and the occupation of the metal e_g levels steadily increases as donation into these orbitals becomes more efficient. Analysis of the metal-based populations of the $1t_{2g}$ and $2t_{2g}$ molecular orbitals is complicated by the increase in formal d-electron count. However, it is clear that the metal-based contribution becomes increasingly located in the lower-lying $1t_{2g}$ orbital in the later haxahalometalates. This can also be seen in the decrease in metal character in the $2t_{2g}$ orbitals, which results in the metal-based population of the $2t_{2g}$ orbitals actually dropping between $[IrX_6]^-$ and $[PtX_6]^-$, despite the formal increase in d-electron count. Similar changes in the $2t_{2g}$ acceptor orbital of neutral hexafluorides have been noted previously and have been used to rationalize the increase in calculated electron afinities from WF_6 ($2t_{2g}$ M−F antibonding) to AuF_6 ($2t_{2g}$ approximately nonbonding and fluoride-based).[9] However, as discussed above, simple inspection of the bonding character of the $2t_{2g}$ orbital fails to rationalize the $[WX_6]^-$ data, and we believe there are difficulties in using this criterion to rationalize the wider trends displayed by the electrochemical and computational results described in this work.[42] We noted above that the lower degree of metal-based electron density in the $2t_{2g}$ orbitals of $[WCl_6]^-$ appeared consistent with its higher electron affinity relative to that of $[WF_6]^-$. In the later $[MX_6]^-$ complexes, this difference between the $[MF_6]^-$ and $[MCl_6]^-$ species becomes more marked (an extra 0.80 e is located on the metal in the $2t_{2g}$ orbitals of $[PtF_6]^-$ compared to that in $[PtCl_6]^-$, while the equivalent difference for the $[WX_6]^-$ pair is only 0.09 e). This would tend to suggest that electron addition to the hexachlorometalates would become relatively easier in the later species. In fact, precisely the opposite trend is seen.

The above analysis highlights the difficulty in selecting a single criterion, or a combination of criteria, to understand the available electron affinity/electrochemical data. As in our previous study,[1] we prefer to adopt a fragmentation approach which allows us to monitor the *total* metal−halide array bonding as a function of the halide, the metal center, and the oxidation state of the metal. Our analysis of the trends in electron affinities computed for $[MX_6]^-$ species will be based on the computation of the energy for the hypothetical process:

$$M^{(z+6)+} + \{X_6\}^{6-} \rightarrow [MX_6]^z$$

$$(M = \text{Ta to Pt; } X = \text{F, Cl; } z = 1-, 2-)$$

This approach requires us to compare several different metal centers, and, as such, it is convenient to consider the formation of $[MX_6]^z$ complexes as a two-step process (see Figure 6). In the first step, we calculate the energies of the $M^{(z+6)+}$ and $\{X_6\}^{6-}$ fragments relative to those of the neutral atoms and the appropriate number of electrons at infinite separation ($E = 0$). For the $\{X_6\}^{6-}$ fragments, we impose the geometry found in the ultimate $[MX_6]^z$ species, while the energies of the M^{5+} and M^{4+} cations were calculated under O_h symmetry with a t_{2g} electron configuration, equivalent to that of the hexahalide complex being studied. The energy change associated with this step is termed the fragment preparation energy. In the second step, these fragments interact to give the final $[MX_6]^z$ complexes. The associated energy change, the metal−halide array interaction energy, does not, therefore, involve any reorganization of the metal t_{2g} electrons.

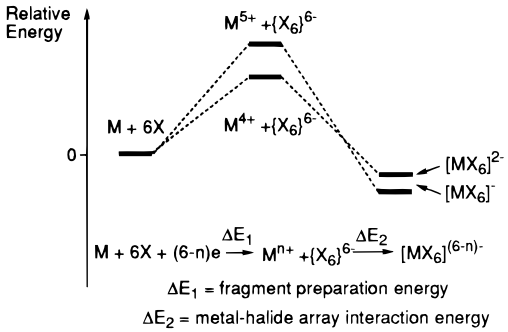

Figure 6. Schematic representation of the formation of $[MX_6]^z$ species from $M^{(n+6)+}$ and $\{X_6\}^{6-}$ fragments (M = Ta to Pt; X = F, Cl; z = 1−, 2−).

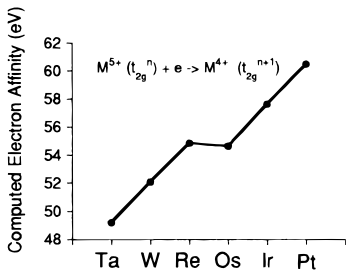

Figure 7. Calculated electron affinities (electronvolts) of free 5d M^{5+} cations in an octahedral environment ($t_{2g}^n + e \rightarrow t_{2g}^{n+1}$, see text for details).

Along the Ta to Pt series, variation in the energy required to form the $\{X_6\}^{6-}$ fragments as they are found in the $[MX_6]^-$ and $[MX_6]^{2-}$ complexes is similar for X = F and Cl. This is consistent with the trends in M−X distances in Table 2, which indicate that, although the lengthening of the metal−halide bond is, in absolute terms, larger upon reduction of an $[MF_6]^-$ species than for its $[MCl_6]^-$ analogue, the relative trend in M−X bond lengthening upon electron addition is similar for both halides from $[TaX_6]^-$ to $[PtX_6]^-$. Changes in inter-halide interactions do not play a significant role in determining the ease of reduction of $[MX_6]^-$ species. We therefore ignore the contribution of the $\{X_6\}^{6-}$ arrays to the fragment preparation energy terms of $[MX_6]^-$ and $[MX_6]^{2-}$ species, which then reduce to the energies required to form the M^{5+} and M^{4+} cations, respectively. The difference in fragment preparation energy for an $[MX_6]^-/[MX_6]^{2-}$ pair is, then, the electron affinity of the free M^{5+} cation and will be common to both the chloride and the fluoride series. Our analysis will, therefore, consider two processes: the electron affinities of free M^{5+} cations and the metal−halide array interaction energies upon formation of the final complexes.

Electron Affinities of Free M^{5+} Cations. The calculated M^{5+} electron affinities (see Figure 7 and Table 6) reaffirm that the general zigzag pattern of the redox data/computed electron

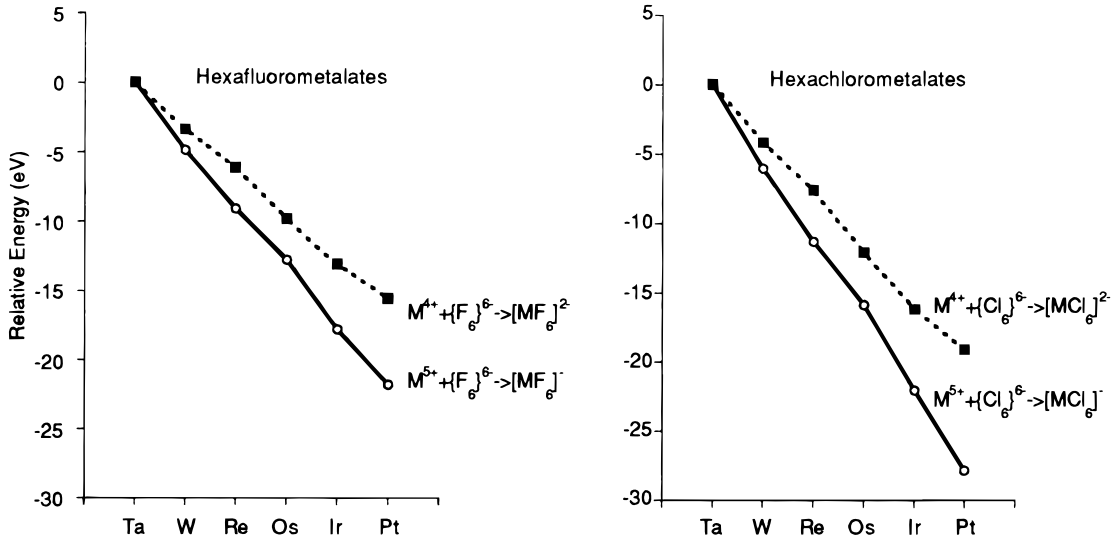

Figure 8. Trends in metal−halide interaction energies for $[MX_6]^{-/2-}$ species (M = Ta to Pt; X = F, Cl). Plots are based on the data presented in Table 7, with the metal−halide interaction energy for $[TaX_6]^{-/2-}$ in each case being set to zero.

Table 6. Computed Electron Affinities (eV) for Free M^{5+} Cations

M	Ta	W	Re	Os	Ir	Pt
electron affinity	49.2	52.1	54.9	54.7	57.6	60.5

Table 7. Metal−Halide Array Interaction Energies (eV) for $[MX_6]^-$ and $[MX_6]^{2-}$ Species (M = Ta to Pt; X = F, Cl)

	Ta	W	Re	Os	Ir	Pt
$[MF_6]^-$	−225.6	−230.6	−234.9	−238.7	−243.7	−247.6
$[MF_6]^{2-}$	−169.5	−173.0	−175.7	−179.5	−182.8	−185.3
$\Delta E(M^V \rightarrow M^{IV})$	56.1	57.6	59.2	59.2	60.9	62.3
$[MCl_6]^-$	−195.1	−201.1	−206.4	−211.0	−217.2	−222.0
$[MCl_6]^{2-}$	−143.2	−147.3	−150.7	−155.3	−159.4	−162.3
$\Delta E(M^V \rightarrow M^{IV})$	51.9	53.8	55.7	55.7	57.8	59.7

affinities arises from placing transition metals in an octahedral environment and assuming maximum spin multiplicity in the t_{2g} orbitals. The increase in electron affinity from Ta^{5+} to Pt^{5+} spans over 11 eV and, again, reflects the increasing core charge of the metal. In contrast, the range in the computed electron affinities of $[MX_6]^-$ complexes is only 4.0 (X = F) and 2.7 eV (X = Cl). The role of the metal core charge, which increasingly favors the lower oxidation state along the Ta to Pt series, is clearly attenuated by the halide array and to a greater extent by the chloride array than by the fluoride array. The next step in our analysis allows us to interpret these different ligand effects in terms of the ability of each halide array to stabilize the two metal oxidation states involved.

Metal−Halide Array Interactions. The metal−halide array interaction energies for $[MX_6]^-$ and $[MX_6]^{2-}$ species (M = Ta to Pt; X = F, Cl) are given in Table 7. For both halides, the metal−halide array interaction is significantly more stabilizing with the higher oxidation state metal center. In general, this counteracts the intrinsic ability of the metal center to accept electrons and results in the computed electron affinities of all the $[MF_6]^-$ and early $[MCl_6]^-$ species being negative (cf. Figure 6). More specifically, we find that, for both metal oxidation states and halides, a steady stabilization of the metal−halide array interaction across the series is computed. This trend is more marked in the higher oxidation state, with the result that $\Delta E(M^V \rightarrow M^{IV})$ in Table 7 increases on moving from $[TaX_6]^{-/2-}$ to $[PtX_6]^{-/2-}$. The effects of the metal−halide array interaction in increasing the stability of the higher oxidation state across the third transition metals acts *against* the trend computed for the electron affinity of free M^{5+} cations, which increasingly favored the lower oxidation state from Ta^{5+} to Pt^{5+}. These two effects, therefore, counteract each other in the electron affinities of $[MX_6]^-$ species, accounting for the smaller range in electron affinity computed from Ta to Pt for the $[MX_6]^-$ complexes compared with that for the free M^{5+} cations. These trends in metal−halide array interaction energies are plotted in Figure 8 and indicate that the relative stabilization of the higher oxidation state metal center increases more rapidly for the hexachlorometalates than for the hexafluorometalates. It is this greater sensitivity of metal−chloride bonding to a change in the metal oxidation state that lies behind the nonparallel, convergent behavior of the reduction potentials of $[MF_6]^-$ and $[MCl_6]^-$ complexes.

Our analysis has been based on the redox data for the $[MX_6]^{-/2-}$ series, as modeled by the computed electron affinities of $[MX_6]^-$ species. Although the electrochemical data set for the $[MX_6]^{0/-}$ series is incomplete, the range of computed electron affinities of MX_6 species is similar to that calculated for $[MX_6]^-$ systems for both X = F and Cl. The arguments developed above for the $[MX_6]^{-/2-}$ series should, therefore, apply equally to the $[MX_6]^{0/-}$ couple, and this proved to be the case. The major difference between the $[MX_6]^{0/-}$ and $[MX_6]^{-/2-}$ series is seen in the gaps in successive couples for X = F and Cl. This is much smaller between the reductions of WF_6 and WCl_6 (0.53 V) than between the reductions of $[WF_6]^-$ and $[WCl_6]^-$ (1.33 V) and is related, in this case, to the wider range of stability of the M^V state in the hexafluorides. Similarly, as illustrated in Figure 1, $[IrF_6]^{2-}$ displays a wider range of stability than $[IrCl_6]^{2-}$. The ability of the hexafluoride array to stabilize these high metal oxidation states over a wider potential range will be discussed elsewhere.[35] In the context of this work, the convergence of the fluoride and chloride series, as modeled by our computed electron affinities, predicts a reversal in the trend of redox data for the neutral hexahalides between WX_6 (X = Cl easier to reduce) and PtX_6 (X = F easier to reduce). Therefore, while WCl_6 does oxidize $[WF_6]^-$, $PtCl_6$ should not oxidize $[PtF_6]^-$.

3. On the Existence of $OsCl_6$, $IrCl_6$, $PtCl_6$, and AuF_6. All the neutral hexafluorides, MF_6 (M = W to Pt), are well-characterized species.[4,5,36] In contrast, of the neutral 5d

(35) Macgregor, S. A.; Moock, K. H., work in progress.
(36) Kimura, M.; Schomaker, V.; Smith, D. W.; Weinstock, B. *J. Chem. Phys.* **1968**, *48*, 4001.

Table 8. Metal Character (%) in Metal−Halide Antibonding t_{2g} Orbitals in MX_6 Species (M = Ta to Pt; X = F, Cl)

	W	Re	Os	Ir	Pt
MF_6	68.2	64.3	58.4	49.6	36.3
MCl_6	58.3	53.8	46.9	36.8	23.3

Table 9. Computed Energies (eV) for the Process $MX_6 \rightarrow MX_4 + X_2$ (M = W to Pt; X = F, Cl)

M	X = F	X = Cl	M	X = F	X = Cl
W	+8.90	+4.00	Ir	+4.99	+1.06
Re	+7.21	+2.70	Pt	+3.36	−0.05
Os	+6.51	+2.18			

hexachlorides, only WCl_6 is well established. $ReCl_6$ has been claimed, but the characterization has been disputed.[37] Our calculations predict that PtF_6 has the highest electron affinity of all the hexahalometalates studied here. In principle, therefore, all the neutral hexachlorides should be accessible through the action of a suitably strong oxidizing agent, for example PtF_6, on the appropriate $[MCl_6]^-$ species.

$$[MCl_6]^- + PtF_6 \rightarrow MCl_6 + [PtF_6]^- \qquad (M = W \text{ to } Pt)$$

Analysis of d-orbital populations in $[MX_6]^-$ species (see Table 5) indicates that one major difference in M−F and M-Cl bonding lies in the extent of halide-to-metal electron donation, with enhanced covalent bonding occurring in the metal−chloride array interaction. This is also reflected in the degree of metal character in the $2t_{2g}$ metal−halide antibonding orbitals in the neutral MX_6 species (Table 8). For a given metal, the greater degree of metal−chloride interaction results in a lower metal character in these orbitals for MCl_6 species. In addition, a drop in metal character occurs with increasing core charge of the metal. For $PtCl_6$, these factors, as well as the high formal oxidation of the metal, result in what are normally considered metal-based t_{2g} orbitals having only 23% metal character. If an electron is removed from $[PtCl_6]^-$, our results suggest that it is the chloride array rather than the metal center which is being oxidized. In other words, the hypothetical $PtCl_6$ may well be unstable with respect to Pt−Cl bond cleavage and formation of Cl_2. The analogous reductive elimination of F_2 from PtF_6 has been observed to occur at elevated temperatures (>260 °C).[38]

To assess these ideas, we have calculated the energy of the following reaction:

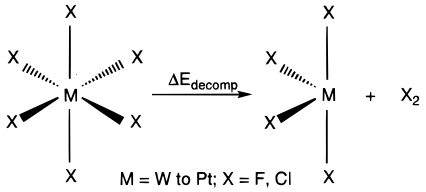

where the C_{2v} MX_4 fragment maintains the geometry found within the octahedral MX_6 species, and the X_2 molecules have been optimized using the same basis set employed for the halide ligands (F−F = 1.404 Å, Cl−Cl = 2.034 Å). Thus, we do not optimize the geometries of the MX_4 species or consider further reaction of what would presumably be a highly reactive species. The calculated energies of this reaction (Table 9), therefore, represent an upper limit for this type of decomposition process.

On this basis, WF_6 and WCl_6 are both stable with respect to loss of X_2, although this process is far less endothermic for the latter. Between W and Pt, this decomposition becomes more favorable for both halides: for PtF_6, $\Delta E_{decomp} = +3.36$ eV, suggesting that loss of F_2 is still highly unlikely at room temperature. These figures are in accord with the known stability of all the 5d MF_6 species (M = W to Pt). In this context, it is interesting to extend the series to consider the stability of the elusive AuF_6.[39] We compute an electron affinity of 7.28 eV for this species, confirming previous findings[7,8a,40] that AuF_6 would be the strongest oxidizing agent of all the transition metal hexafluorides studied here. In addition, we calculate AuF_6 to be thermodynamically stable with respect to formation of d^7 AuF_4 and F_2 ($\Delta E_{decomp} = +1.91$ eV). For the MCl_6 species, the decomposition process remains endothermic from W to Ir. However, for $PtCl_6$, loss of Cl_2 is, in fact, slightly exothermic ($\Delta E_{decomp} = -0.05$ eV). These considerations indicate that $OsCl_6$ and $IrCl_6$ are more likely to be stable than $PtCl_6$. In future work, we shall attempt to generate these species by using electrochemical methods.

Conclusions

(1) Trends in experimental redox data for $[MX_6]^{z/z-1}$ (M = Ta to Pt; X = F, Cl; $z = 0, 1-$) systems have been modeled by computation of the electron affinities of $[MX_6]^z$ species. For a given isovalent series, both the nonlinear zigzag progression and the convergence of redox data for analogous fluoro and chloro series are reproduced by our calculations.

(2) The trends in redox data have been rationalized computationally in terms of a fragmentation approach in which the central metal cation interacts with the halide array. The zigzag trend in redox data across the third row transition metal hexahalometalates reflects the increase in metal core charge and the octahedral symmetry of these species, which results in electron pairing for d-electron counts greater than 3. The role of the metal core charge is attenuated to different extents by the fluoride and chloride arrays. For a given $[MX_6]^{z/z-1}$ isovalent series, both halides exhibit an increased ability to stabilize the higher metal oxidation state in the later metals. This effect is greater for chloride and leads to the observed convergence of the redox data for isovalent hexafluoro- and hexachlorometalate series.

(3) The stability of the unknown 5d metal hexachlorides with respect to Cl_2 loss is predicted to follow the order $OsCl_6 > IrCl_6 > PtCl_6$.

Acknowledgment. This work was carried out in the laboratory of Dr. G. A. Heath and was supported by the Institute of Advanced Studies, ANU. We thank Dr. Heath for useful discussions. K.H.M. thanks the government-sponsored R&D syndicate (Tetley Manufacturing Ltd., Sydney, Australia) for financing his position at ANU. We also thank Prof. M. A. Bennett for a critical review of our manuscript.

IC9605736

(37) Burgess, J.; Fraser, C. J. W.; Haigh, I.; Peacock, R. D. *J. Chem. Soc., Dalton Trans.* **1973,** 501 and references therein.
(38) Weinstock, B.; Malm, J. G.; Weaver, E. E. *J. Am. Chem. Soc.* **1961**, *83*, 4310.
(39) *Gmelin Handb.* Au Suppl., **1992**, *B1*, pp 158−159.
(40) Miyoshi, E.; Sakai, Y. *J. Chem. Phys.* **1988**, *89*, 7363.
(41) Magnuson R. H. *Inorg. Chem.* **1984**, *23*, 387.
(42) For example, the percentage metal character of the $2t_{2g}$ acceptor orbitals of $[PtF_6]^-$ and $[PtCl_6]^-$ is 42.9% and 27.0%, respectively. In this case, the chloride has the higher computed electron affinity. For PtF_6 and $PtCl_6$, the percentage metal characters of the $2t_{2g}$ orbitals are 36.3% and 23.3%, respectively, although the neutral hexafluoride now has the greater electron affinity. Relatively small changes in percentage metal character, therefore, lead to dramatic shifts in the relative electron acceptor abilities of these hexahalometalates, and it is difficult to provide a quantitative rationalization of this on the basis of the percentage metal characters of the acceptor orbitals involved.